Supplementary Information

PUMA Binding Induces Partial Unfolding within BCL-xL to Disrupt p53 Binding and Promote Apoptosis

Ariele Viacava Follis[1]*, Jerry E. Chipuk[2*#], John C. Fisher[1,4]*, Mi-Kyung Yun[1], Grace Royappa[1], Amanda Nourse[3], Christy R. Grace[1], Katherine Baran[2], Li Ou[1] Lie Min[1], Stephen W. White[1,5], Douglas R. Green[2,6] ** and Richard W. Kriwacki[1,5,6] **

[1]Department of Structural Biology

[2]Department of Immunology

[3]Hartwell Center for Bioinformatics and Biotechnology

St. Jude Children's Research Hospital, 262 Danny Thomas Place, Memphis, Tennessee, USA 38105

[4]College of Medicine

[5]Department of Microbiology, Immunology and Biochemistry

University of Tennessee Health Sciences Center, Memphis, Tennessee, USA 38163

[#]Current Affiliation: Department of Oncological Sciences, One Gustave L. Levy Place, New York, New York, USA 10029

*,** These authors contributed equally.

[6]Corresponding authors information:

D.R.G.: phone (901) 595-3488, e-mail douglas.green@stjude.org

R.W.K.: phone (901) 595-3290, e-mail richard.kriwacki@stjude.org

Inventory of Supplementary Information

Supplementary Figure 1

Supplementary Figure 2

Supplementary Figure 3 is related to Figure 2

Supplementary Figure 4

Supplementary Figure 5 is related to Figure 2

Supplementary Figure 6 is related to Figure 2

Supplementary Figure 7 is related to Figure 2

Supplementary Figure 8 is related to Figure 2

Supplementary Figure 9 is related to Figure 2

Supplementary Figure 10 is related to Figure 2

Supplementary Figure 11 is related to Figure 2

Supplementary Figure 12

Supplementary Figure 13 is related to Figure 3

Supplementary Figure 14 is related to Figure 4

Supplementary Figure 15 is related to Figure 4

Supplementary Figure 16 is related to Online Methods

Supplementary Figure 17 is related to Online Methods

Supplementary Figure 18 is related to Figures 3,4

Supplementary Table 1 is related to Figure 1

Supplementary Table 2 is related to Figure 2

Supplementary Table 3 is related to Supplementary Figure 4a

Supplementary Table 4 is related to Supplementary Figure 4b

Supplementary Table 5 is related to Figure 2

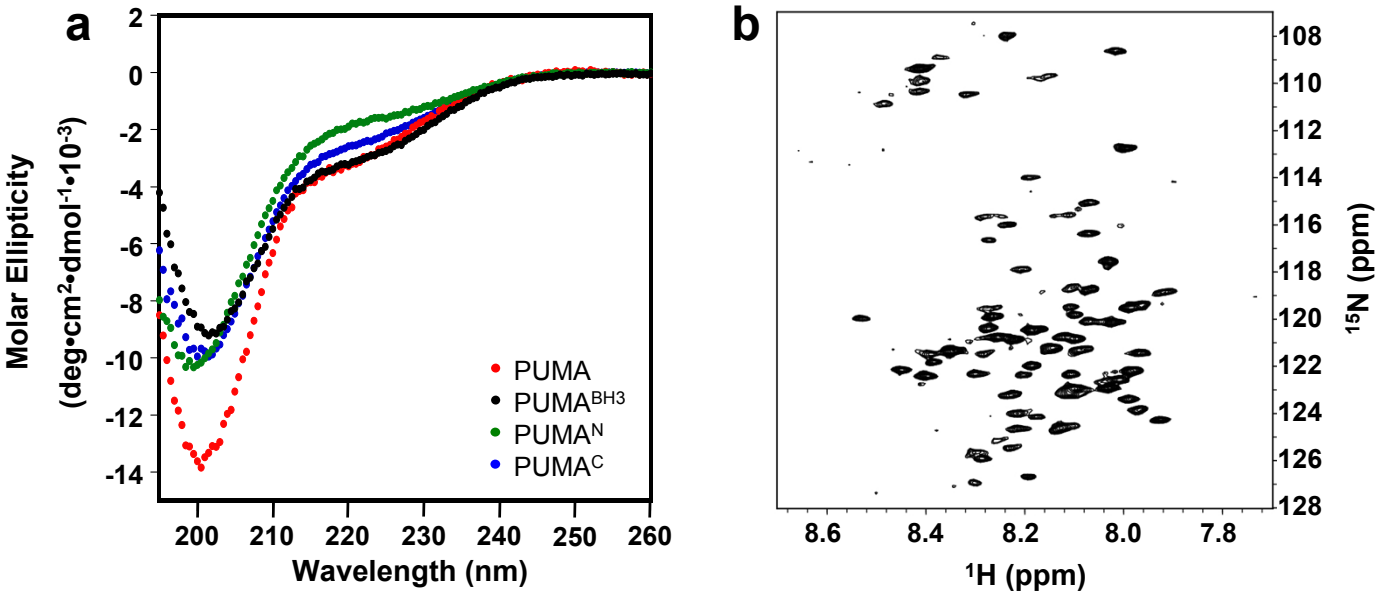

Supplementary Figure 1. PUMA is disordered. **a.** PUMAβ (hereafter referred to as PUMA) is a disordered protein. The circular dichroism (CD) spectrum of PUMA exhibited a minimum value of molar ellipticity at 200 nm, consistent with a lack of highly populated secondary structure. A weak feature at 222 nm indicated nascent α-helical secondary structure that can be attributed to the PUMA BH3 domain ($PUMA^{BH3}$) by comparison of CD spectra for PUMA and those for $PUMA^{BH3}$ and amino and carboxyl terminal fragments of PUMA lacking the BH3 domain ($PUMA^{N}$ and $PUMA^{C}$, respectively). **b.** The 2D ^{1}H-^{15}N HSQC spectrum of PUMA exhibited the appropriate number of resonances; however, the peaks were dispersed over a narrow ^{1}H chemical shift range (≤ 1 ppm) indicating that PUMA is disordered.

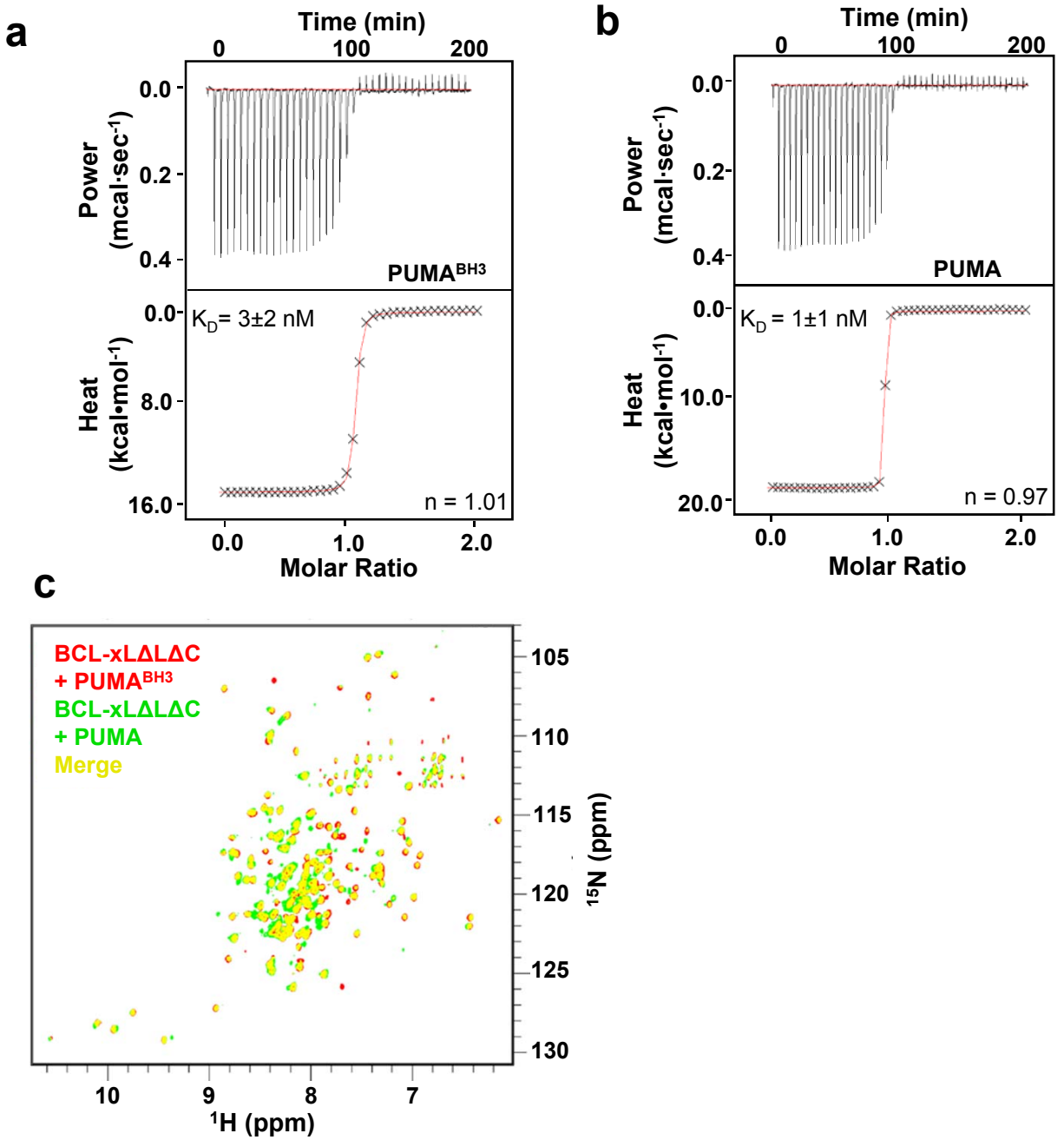

Supplementary Figure 2. The PUMA BH3 domain is sufficient for binding BCL-xL. **a-b.** ITC binding isotherms recorded for BCL-xLΔC (functional, recombinant BCL-xL lacking the carboxyl terminal 22 residues)[1] titrated into a solution of $PUMA^{BH3}$ (**a**) or PUMA (**b**); $PUMA^{BH3}$ and PUMA yielded nearly identical, low nanomolar K_D values for binding to BCL-xLΔC. Errors represent the standard deviation calculated from at least two independent experiments. **c.** The ^{1}H-^{15}N TROSY spectrum of a functional BCL-xL protein lacking the unstructured loop connecting α-helix 1 (α1) to α2 as well as the carboxyl terminal 22 residues, termed BCL-xLΔLΔC[1] shows similar perturbation patterns upon addition of either $PUMA^{BH3}$ (red colored peaks) or PUMA (green colored peaks). The red and green colors combine to give yellow when superimposed. The extensive appearance of yellow peaks indicates the high degree of similarity between the red and green colored spectra.

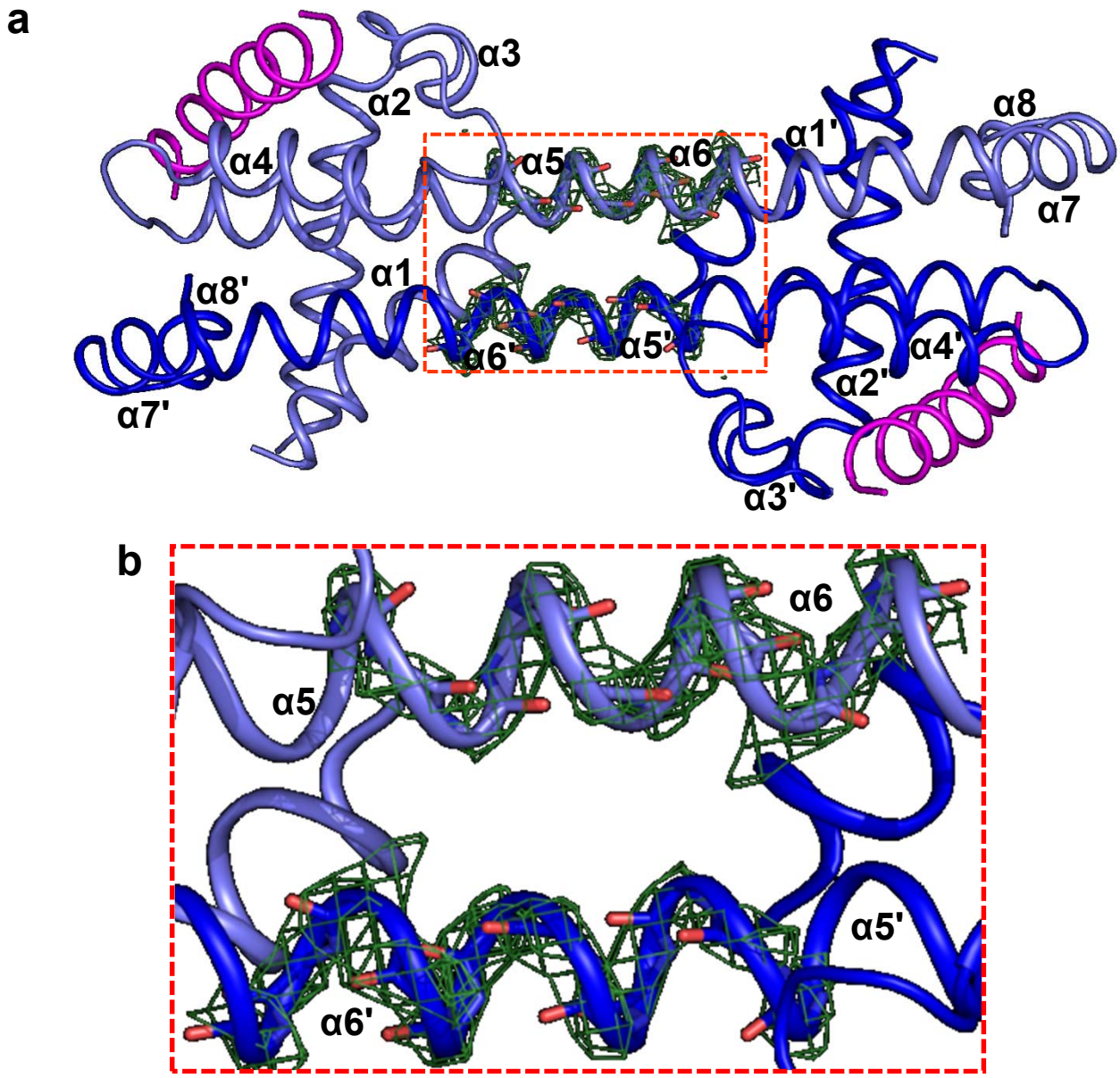

Supplementary Figure 3. The BCL-xLΔC•PUMA^{BH3} complex forms a domain-swapped dimer in crystals. **a-b.** A view of the electron density and BCL-xLΔC domain-swapped dimer model in the region that mediates domain swapping. **a**. A view of the entire domain-swapped dimer; the region highlighted with a red box in **a** is expanded in **b** to illustrate the continuity of electron density for α5 and α6 across the dimer interface. The two copies of the PUMA BH3 peptide are illustrated in magenta in **a**.

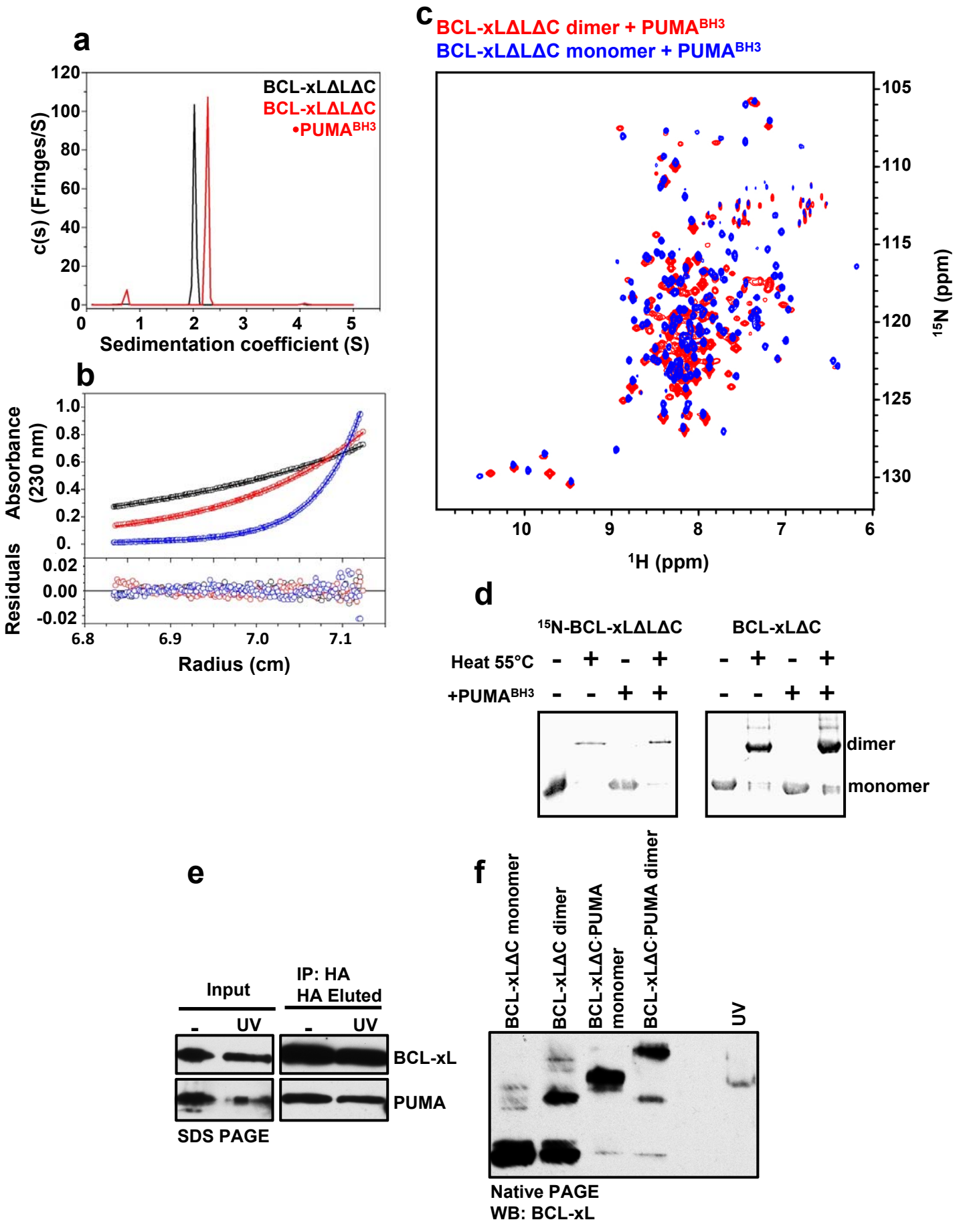
a
BCL-xLΔLΔC
BCL-xLΔLΔC
•PUMA^BH3
c(s) (Fringes/S)
Sedimentation coefficient (S)
b
Absorbance (230 nm)
Residuals
Radius (cm)
c
BCL-xLΔLΔC dimer + PUMA^BH3
BCL-xLΔLΔC monomer + PUMA^BH3
^1H (ppm)
^15N (ppm)
d
^15N-BCL-xLΔLΔC
BCL-xLΔC
Heat 55°C
+PUMA^BH3
dimer
monomer
e
Input
IP: HA
HA Eluted
UV
BCL-xL
PUMA
SDS PAGE
f
BCL-xLΔC monomer
BCL-xLΔC dimer
BCL-xLΔC·PUMA monomer
BCL-xLΔC·PUMA dimer
UV
Native PAGE
WB: BCL-xL

Supplementary Figure 4 (previous page). The form of the BCL-xLΔLΔC·PUMA^{BH3} complex in solution exhibits 1:1 stoichiometry *in vitro* and in cells. **a-b**. Sedimentation velocity and equilibrium analytical ultracentrifugation experiments indicate that the complex of BCL-xLΔLΔC bound to PUMA^{BH3} displays 1:1 stoichiometry. Sedimentation velocity experiment (**a**) : free BCL-xLΔLΔC (black trace); BCL-xLΔC•PUMA^{BH3} (red trace). Equilibrium experiment (**b**): absorbance profile plotted against the distance from the axis of rotation for 1.4 μM BCL-xLΔC•PUMA^{BH3} centrifuged at 12800 (black), 17400 (red) or 30000 rpm (blue). **c**. 2D ^{1}H-^{15}N TROSY spectra of ^{15}N apo monomeric BCL-xLΔLΔC (blue colored peaks) or apo, domain-swapped dimeric BCL-xLΔLΔC (red colored peaks) to which PUMA^{BH3} peptide was added. These samples with ^{15}N-labeled BCL-xLΔLΔC were prepared in the same manner as those prepared in unlabeled form and analyzed using AUC (Suppl. Fig. 1), which showed that the monomeric sample remained monomeric upon PUMA^{BH3} addition, and that the dimeric sample remained dimeric. The spectrum of apo, domain-swapped dimeric ^{15}N-BCL-xLΔLΔC was essentially identical to that reported previously by Denisov, et al.[2] **d**. Native polyacrylamide gel electrophoresis (PAGE) analysis showing formation of apo domain-swapped dimeric ^{15}N-BCL-xLΔLΔC and BCL-xLΔC upon treatment at 55°C (heat 55 °C), but not upon addition of PUMA^{BH3} at 25 °C (+PUMA^{BH3}). The analyzed samples contained 50 μM BCL-xL (in monomer concentration) and a 1.2 molar excess of PUMA^{BH3} peptide (when present). The apo domain-swapped dimeric ^{15}N-BCL-xLΔLΔC species was separated from residual monomers by gel filtration chromatography prior to NMR analysis. **e**. SDS PAGE and western blot analysis of BCL-xL and PUMA in MCF7 cells expressing HA-tagged BCL-xL treated with or without UV (100 mJ/cm^2). Protein levels in whole cell extracts are compared with HA-immunoprecipitated and HA-eluted protein. **f.** Native PAGE and BCL-xL western blot analysis of HA-eluted protein from UV treated cells compared with monomeric BCL-xLΔC, dimeric BCL-xLΔC, monomeric BCL-xLΔC·PUMA (1:1) and dimeric BCL-xLΔC·PUMA (2:2) complex standards.

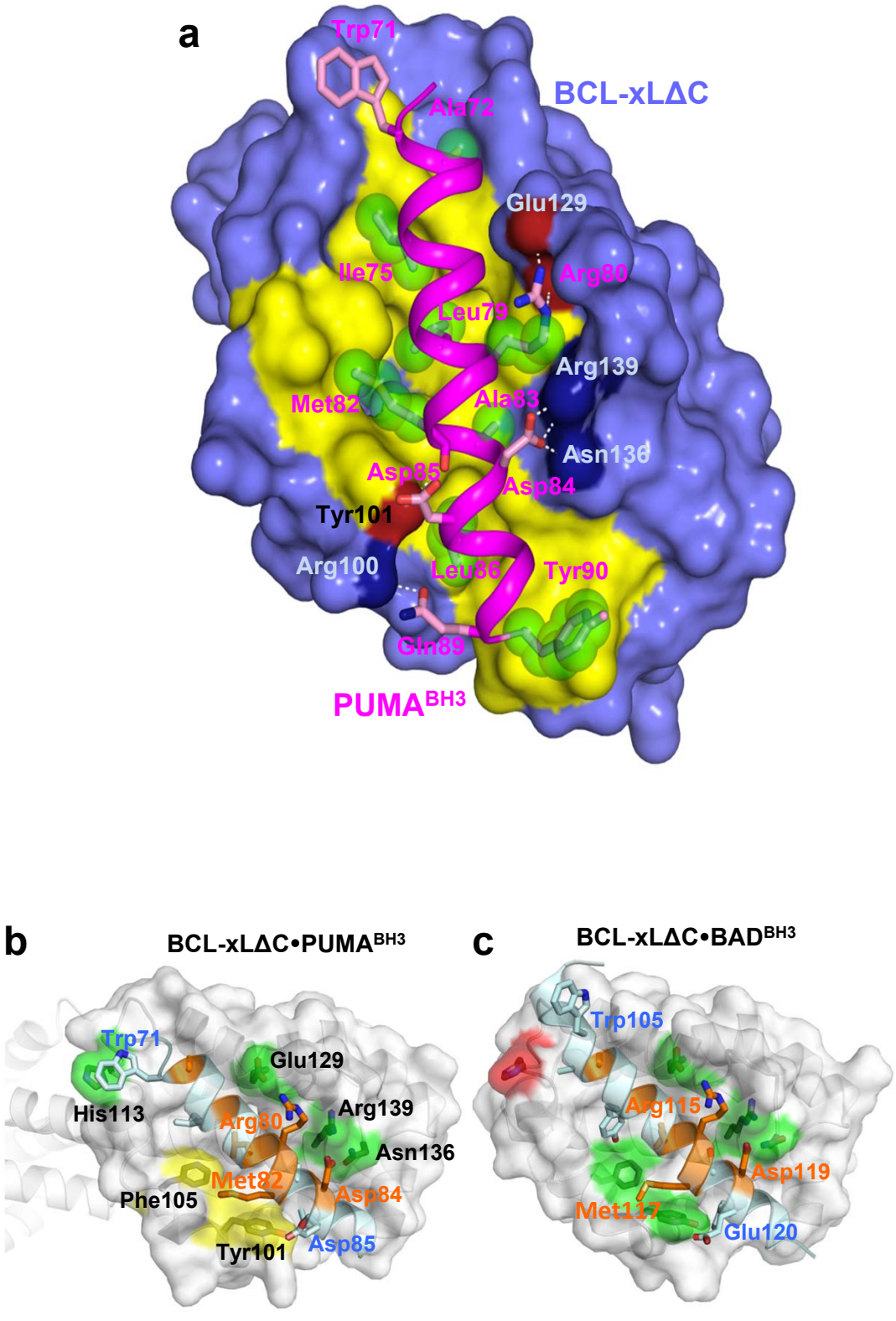
a
Trp71
Ala72
BCL-xLΔC
Glu129
Ile75
Arg80
Leu79
Arg139
Met82
Ala83
Asn136
Asp85
Asp84
Tyr101
Arg100
Leu86
Tyr90
Gln89
PUMA BH3
b
BCL-xLΔC•PUMA BH3
Trp71
Glu129
His113
Arg80
Arg139
Asn136
Met82
Asp84
Phe105
Tyr101
Asp85
c
BCL-xLΔC•BAD BH3
Trp105
Arg115
Asp119
Met117
Glu120

Supplementary Figure 5 (previous page). The PUMA^{BH3} peptide binds BCL-xLΔC through interactions observed in other BH3 domain complexes[3-6]. **a**. For example, the side chains of the conserved Leu^{79}, and, to a lesser extent those of Ile^{75} and Met^{82}, reside deeply within the hydrophobic groove formed between α4 and α5 of BCL-xL; Arg^{80} is engaged in an electrostatic interaction with BCL-xL Glu^{129}; the small side-chain of Ala^{83} is required to avoid steric clashes with α5 of BCL-xL, and the conserved Asp^{84} residue is engaged in an electrostatic interaction with the side-chain of BCL-xL Arg^{139}. These residues of PUMA^{BH3} are highlighted in Fig. 1b. However, Trp^{71} is unique within the PUMA BH3 domain and mediates an unique interaction with His^{113} of BCL-xL. **b-c.** The network of interactions connecting α3 of BCL-xL to PUMA^{BH3} and other portions of the BCL-xL folded core (**b**) is only partially formed compared to the BCL-xL·BAD^{BH3} complex (PDB: 2BZW) (**c**). Residues within the BH3 domain that are identical in PUMA^{BH3} and BAD^{BH3} are colored in orange. Residues within BCL-xL involved in interactions with PUMA^{BH3} or BAD^{BH3} that are well-established, partially formed, or missing are colored in green, yellow and red respectively. While interactions between the two BH3 peptides and α4 - α5 of BCL-xL are quite similar (*e.g.*, interactions between BCL-xL Glu^{129} and PUMA Arg^{80} or BAD Arg^{115}; BCL-xL Asn^{136} and Arg^{139}, and PUMA Asp^{84} or BAD Asp^{119}), interactions between each BH3 peptide and α3 of BCL-xL display several differences. The π-stacking between BCL-xL His^{113} and PUMA Trp^{71} is not observed for BAD Trp^{105}, which is shifted one position towards the N-terminus of the BH3 α-helix compared to PUMA Trp^{71}. The network of hydrophobic interactions involving BCL-xL Phe^{105} and PUMA Leu^{79} and Met^{82}, or BAD Leu^{114} and Met^{117} is different between the two complexes. For example, the sidechain of BCL-xL Phe^{105} is shifted away from residues within α5 in the BCL-xLΔC·PUMA^{BH3} complex. Lastly, a hydrogen bond between the sidechains of BCL-xL Tyr^{101} and BAD Glu^{120} fails to form between BCL-xL Tyr^{101} and PUMA Asp^{85}.

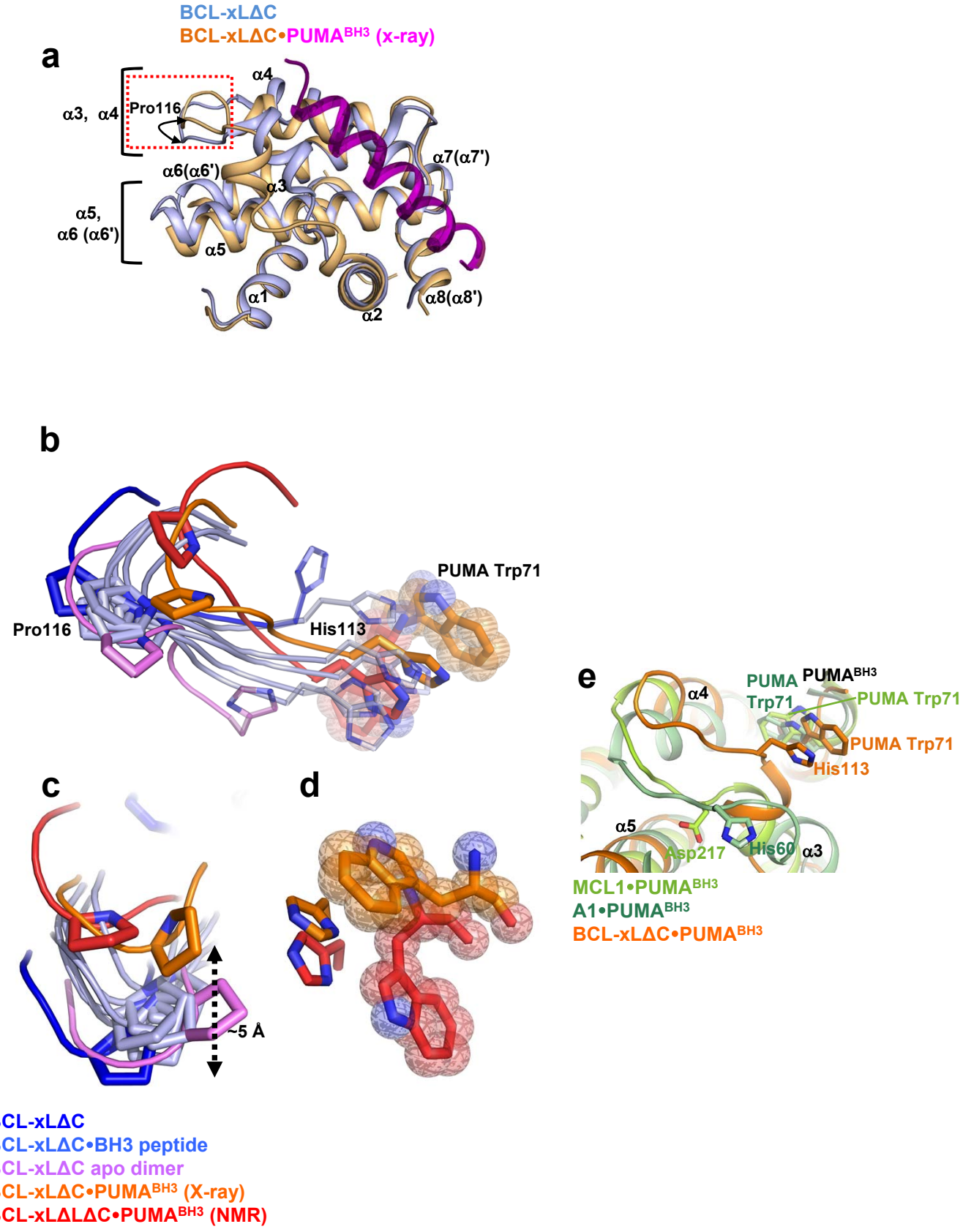
BCL-xLΔC
BCL-xLΔC•PUMA^BH3 (x-ray)
a
α4
α3, α4
Pro116
α7(α7')
α6(α6')
α3
α5,
α6 (α6')
α5
α1
α2
α8(α8')
b
PUMA Trp71
Pro116
His113
c
d
~5 Å
e
PUMA
Trp71
PUMA^BH3
α4
PUMA Trp71
PUMA Trp71
His113
α5
Asp217
His60
α3
MCL1•PUMA^BH3
A1•PUMA^BH3
BCL-xLΔC•PUMA^BH3
BCL-xLΔC
BCL-xLΔC•BH3 peptide
BCL-xLΔC apo dimer
BCL-xLΔC•PUMA^BH3 (X-ray)
BCL-xLΔLΔC•PUMA^BH3 (NMR)

Supplementary Figure 6 (previous page). The binding of PUMA^{BH3} perturbs the structure of the helical core of BCL-xL in the context of the domain-swapped dimer observed in crystals. **a**. Alignment of the structure of one globular core of the domain-swapped dimeric BCL-xLΔC·PUMA^{BH3} complex (orange) and that of apo BCL-xLΔC (PDB: 1R2D; blue) which illustrates the displacement of the loop between α3 and α4 toward the PUMA^{BH3} peptide. **b-c**. Two close-up views of the α3-α4 loop region of BCL-xL, as illustrated in **a**, also including alignment of the BCL-xLΔLΔC·PUMA^{BH3} solution structure, several other BCL-xL·BH3 domain complexes [BAD,2BZW;, BIM,1PQ1; Beclin1,2P1L; BAX,3PL7; and BAK,1BXL (all are colored in light violet for simplicity)], as well as the structure of the domain-swapped dimer of BCL-xL in its apo form (PDB: 2B48; purple), highlighting the displacement of BCL-xL Pro^{116} induced upon binding of PUMA^{BH3}. **d**. Detail of the interaction between PUMA Trp^{71} and BCL-xL His^{113} [in the x-ray (orange) and solution structures (red) of the complex] that is associated with the displacement of BCL-xL Pro^{116}. In the NMR structure of the complex, the sidechain of PUMA Trp^{71} (red) is rotated toward α3 of BCL-xLΔC and more deeply buried within the protein-peptide interface compared to the crystal structure (orange). **e**. Structure alignment between BCL-xLΔC·PUMA^{BH3} (orange), MCL1·PUMA^{BH3} (PDB: 2ROC; light green) and A1·PUMA^{BH3} (PDB: 2VOF; dark green) complexes, highlighting the same region displayed in **b**. The interaction between BCL-xL His^{113} and PUMA Trp^{71} is not observed between the corresponding residues in the other structures (PUMA Trp^{71}, MCL1 Asp^{217} or A1 His^{60}). Correspondingly, the loop connecting α-helices 3 and 4, displaced in BCL-xL upon PUMA binding, fails to shift in both MCL1 and A1.

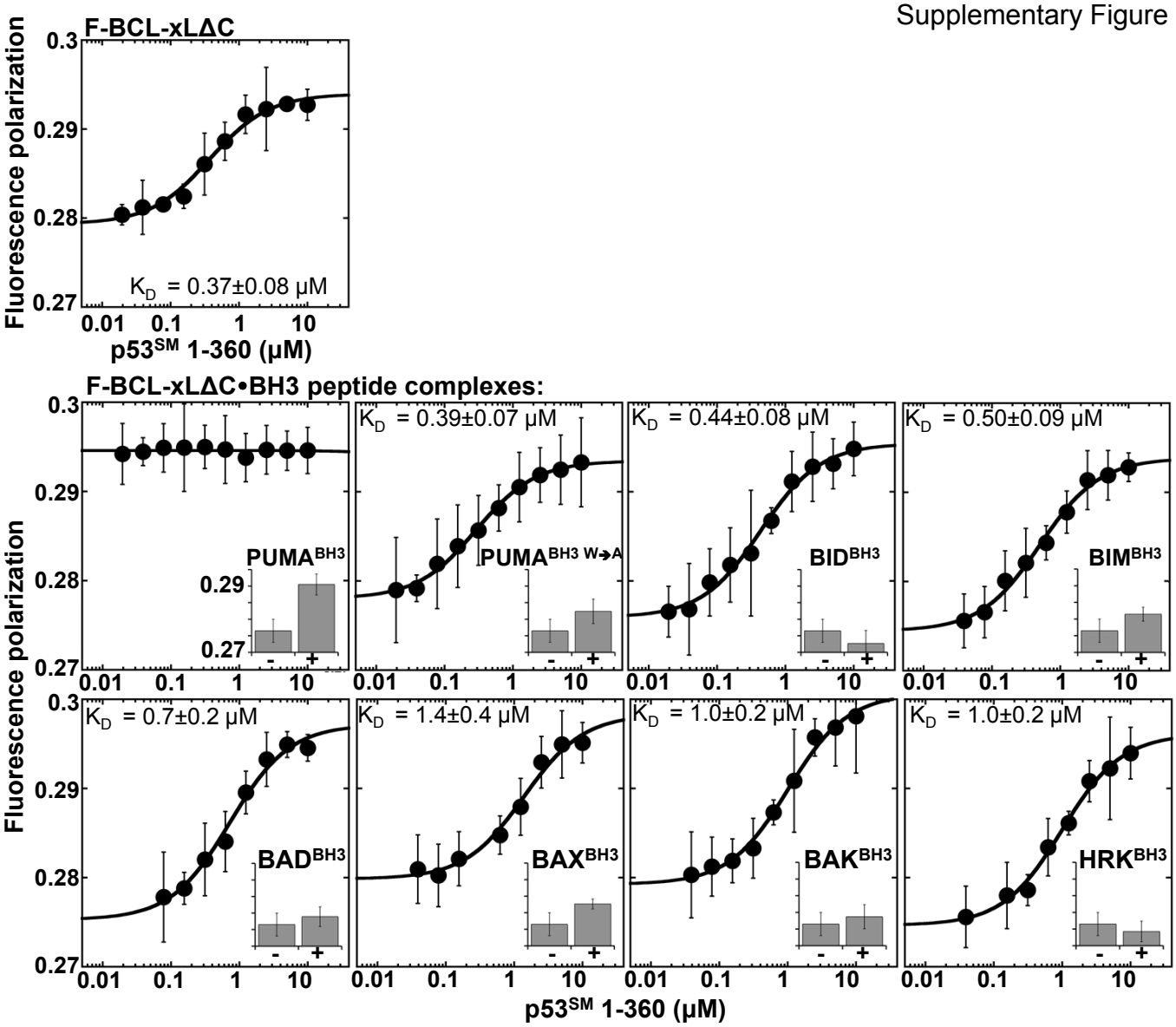

Supplementary Figure 7. Analysis of the binding of $p53^{SM}$ 1-360 to apo BCL-xLΔC and BCL-xLΔC pre-incubated with the indicated BH3 domain peptides using fluorescence polarization. Cys^{151} of BCL-xLΔC was mutated to Ser and Ser^{2} was mutated to Cys to allow fluorescent labeling with fluorescein (F-BCL-xLΔC; used at 100 nM in all experiments); pre-incubation was performed in the presence of 200 nM BH3 domain peptides. These concentrations ensured complete formation of each F-BCL-xLΔC·BH3 complex based on K_D values for the various BH3 peptides for BCL-xLΔC determined using ITC titrations (Suppl. Table 5); these K_D values ranged from 0.2 nM to 120 nM. Changes in fluorescence polarization induced by peptide binding ("+" versus "-"), prior to the p53 titration, are indicated as bar plots in the insets. We reasoned that binding of the small BH3 peptides (~3 KDa) to F-BCL-xLΔC (~24 KDa) does not result in decreased overall tumbling of the labeled BCL-xLΔC. These variations were measured to monitor local dynamic changes of the fluorophore within F-BCL-xL upon peptide binding, which may give rise to some change in polarization values, and are not indicative of the extent of binding of the various peptides. The data are representative of 5 independent experiments and were fit to a 1:1 binding Langmuir isotherm equation; error bars represent the standard error of the mean.

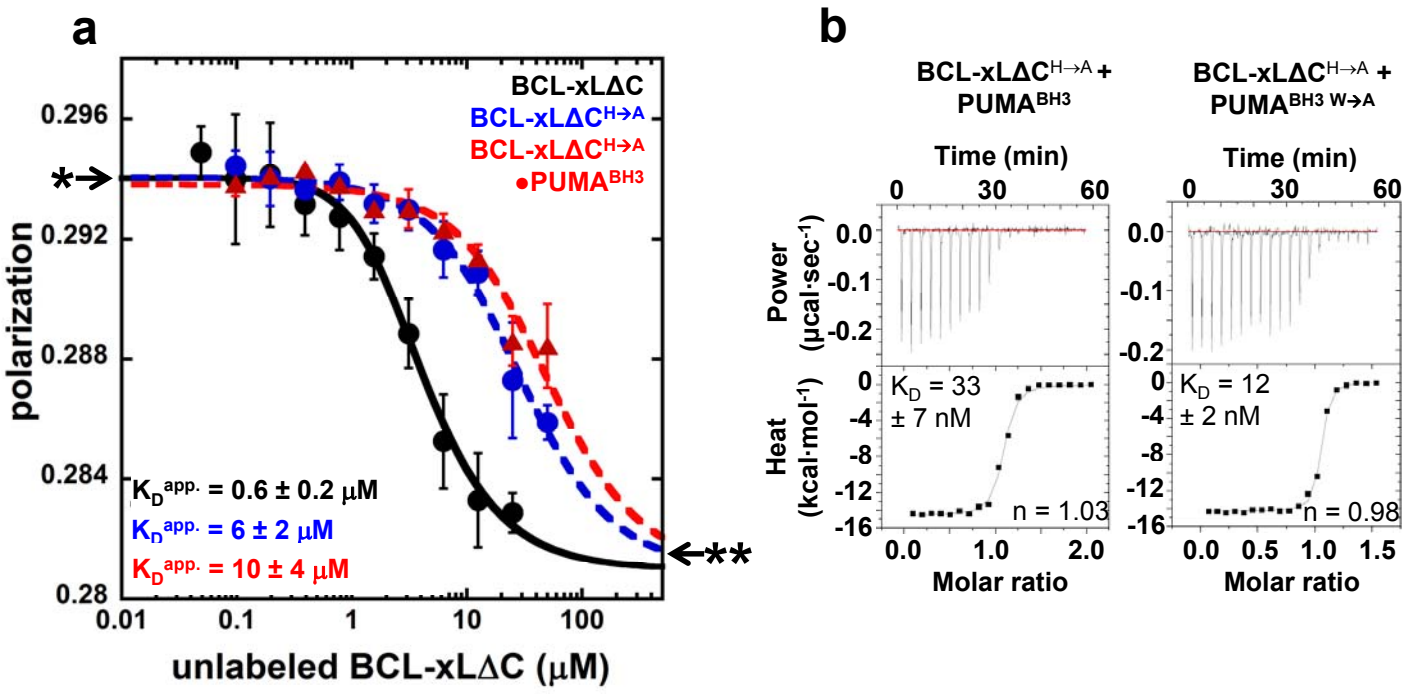

F-BCL-xLΔC•p53^SM 1-360 complex

Displaced F-BCL-xLΔC

Supplementary Figure 8. His^{113} of BCL-xL is required for Trp^{71} of PUMA to induce unfolding of BCL-xL α2- α3 via a π-stacking interaction. **a**. Fluorescence polarization competition titrations between F-BCL-xLΔC and unlabeled BCL-xLΔC (black), BCL-xLΔC$^{H\rightarrow A}$ (blue) or BCL-xLΔC$^{H\rightarrow A}$ ·PUMA^{BH3} (red) for binding p53^{SM} 1-360. The binding of unlabeled BCL-xL to p53 results in release of the labeled protein and a consequent decrease of its fluorescence polarization. The concentration of F-BCL-xLΔC and p53^{SM} 1-360 was 100 nM and 1 μM respectively and was kept constant throughout the titration points. Error bars represent the standard error of the mean of three independent titrations. For the competition experiment with BCL-xLΔC$^{H\rightarrow A}$ •PUMA^{BH3}, a slight molar excess of BCL-xLΔC$^{H\rightarrow A}$ (50 μM) was incubated with 48 μM PUMA^{BH3} (to ensure the absence of free PUMA ^{BH3}) prior to performing serial dilutions in the presence of F-BCL-xLΔC and p53^{SM} 1-360. The fluorescence polarization values were measured within 3 minutes of sample mixing. Since compexes between BCL-xL and BH3 peptides are characterized by a slow dissociation rate, these precautions assured that the extent of PUMA^{BH3} binding to F-BCL-xLΔC, which would bias the experimental outcome, was kept to a minimum during the time required to collect the data. Binding between BCL-xL and p53, on the other hand, exhibits fast to intermediate exchange rates in NMR experiments. A short incubation time is therefore sufficient to observe competition between the fluorescently labeled and unlabeled BCL-xL components for binding p53.**b**. ITC binding isotherms for PUMA^{BH3} and PUMA$^{BH3\ W\rightarrow A}$ binding to BCL-xLΔC$^{H\rightarrow A}$. This mutant form of BCL-xL binds both peptides with high affinity, although the K_D values are slightly higher compared to the wild type protein.

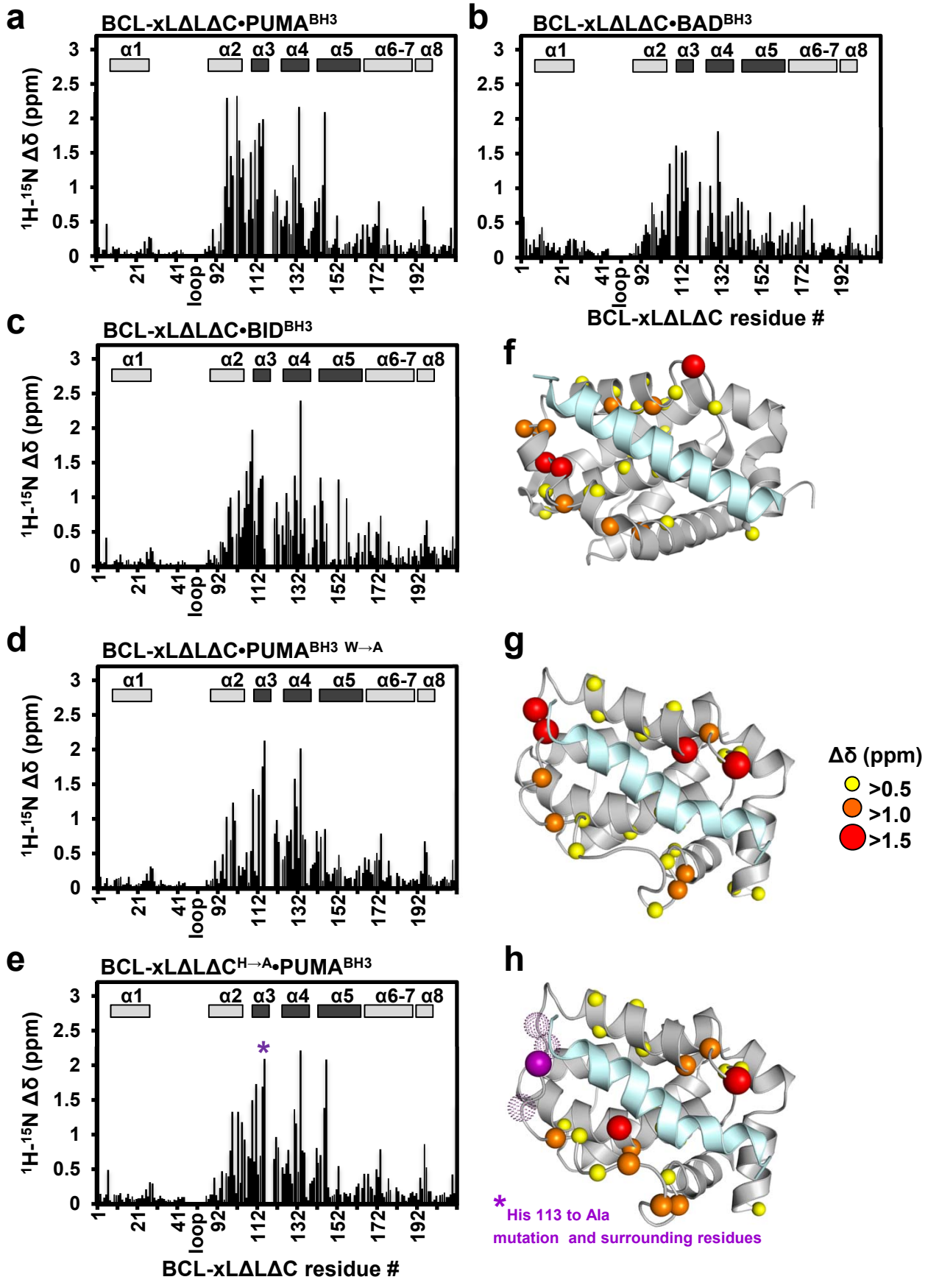
a
BCL-xLΔLΔC•PUMA^BH3
b
BCL-xLΔLΔC•BAD^BH3
c
BCL-xLΔLΔC•BID^BH3
d
BCL-xLΔLΔC•PUMA^BH3 W→A
e
BCL-xLΔLΔC^H→A•PUMA^BH3
f
g
h
α1
α2
α3
α4
α5
α6-7
α8
loop
1H-15N Δδ (ppm)
BCL-xLΔLΔC residue #
Δδ (ppm)
>0.5
>1.0
>1.5
* His 113 to Ala mutation and surrounding residues

Supplementary Figure 9 (previous page). $PUMA^{BH3}$ binding induces local unfolding and dynamics within the BCL-xL structure to a greater extent than do BH3 domains of other BH3 only proteins. ^{1}H-^{15}N NMR chemical shift perturbation analysis of structural and dynamic perturbation for ^{15}N-BCL-xLΔLΔC upon complexation with a slight molar excess of $PUMA^{BH3}$ (**a**), BAD^{BH3} (**b**), BID^{BH3} (**c**) and $PUMA^{BH3\ W\rightarrow A}$ (**d**) or ^{15}N-BCL-xLΔLΔ$C^{H\rightarrow A}$ in complex with $PUMA^{BH3}$ (**e**). The chemical shift perturbation in the latter case is determined by comparison with resonances of free wild type BCL-xLΔLΔC; the position of the His^{113} to Ala mutation is highlighted with a purple asterisk. The chemical shift perturbation data illustrated in **a-b** are mapped onto the respective structures in Fig.1 d-e. The data illustrated in **c** are mapped onto the BCL-xLΔLΔC·BIM^{BH3} structure (PDB: 1PQ1) in **f**; the data illustrated in **d** and **e** are mapped onto the BCL-xLΔLΔC·$PUMA^{BH3}$ structure in **f** and **g,** respectively.

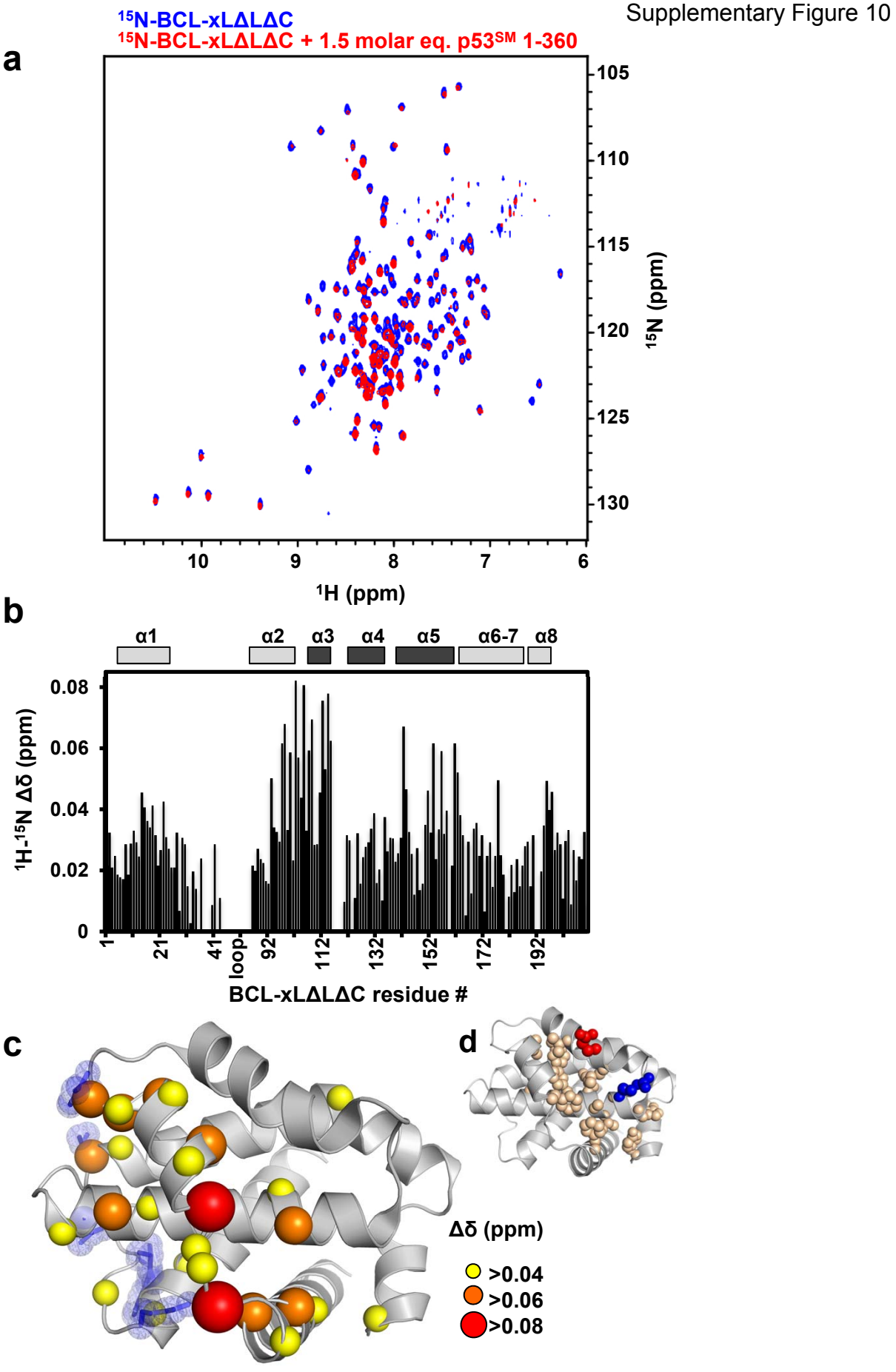
a
15N-BCL-xLΔLΔC
15N-BCL-xLΔLΔC + 1.5 molar eq. p53SM 1-360
105
110
115
120
125
130
15N (ppm)
10
9
8
7
6
1H (ppm)
b
α1
α2
α3
α4
α5
α6-7
α8
0.08
0.06
0.04
0.02
0
1H-15N Δδ (ppm)
1
21
41
loop
92
112
132
152
172
192
BCL-xLΔLΔC residue #
c
d
Δδ (ppm)
>0.04
>0.06
>0.08

Supplementary Figure 10 (previous page). p53 binds to a surface of BCL-xLΔLΔC that does not overlap with the BH3 binding groove. **a**. ^{1}H-^{15}N NMR chemical shift perturbation of ^{15}N-BCL-xLΔLΔC upon binding by $p53^{SM}$ 1-360: 2D ^{1}H-^{15}N TROSY spectra of ^{15}N-BCL-xLΔLΔC were recorded in the absence (blue colored peaks) and presence (red colored peaks) of a 1.5 molar excess of $p53^{SM}$ 1-360. **b**. ^{1}H-^{15}N NMR chemical shift perturbation analysis of the data presented in **a** for $p53^{SM}$ 1-360 binding to ^{15}N-BCL-xLΔLΔC. **c**. Illustration of the data in **b** in the context of the structure of BCL-xLΔC (PDB: 1R2D). The colored spheres centered at Cα atoms illustrate the magnitude of ^{1}H-^{15}N $\Delta\delta$ values, as follows: red, $\Delta\delta \geq 0.08$ ppm; orange, $\Delta\delta = 0.06$-0.08; yellow, $\Delta\delta = 0.04$-0.06. The semi-transparent spheres colored in blue illustrate ^{1}H-^{13}C sidechain chemical shift perturbations, reported by Petros, et al.[7], upon binding of the p53 DNA binding domain to isotopically labeled BCL-xLΔLΔC. **d.** Ilustration of hydrophobic residues (light brown) involved in the interaction between BCL-xL and BH3 peptides. The charged residues Glu^{129} (red) and Arg^{137} (blue), critical for BH3 binding, are also displayed. The orientation of BCL-xL is the same as in **c**.

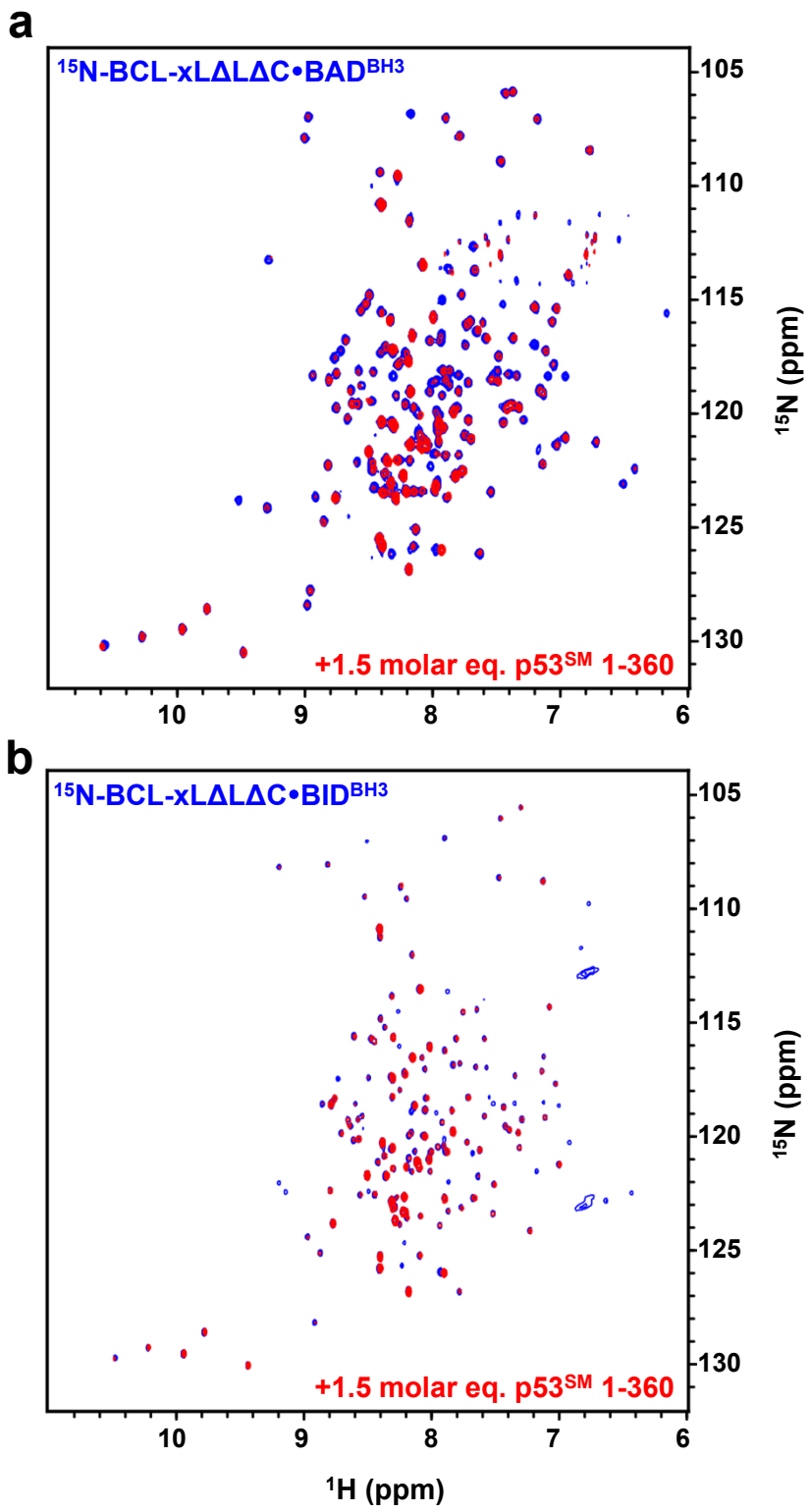

Supplementary Figure 11. NMR analysis confirms the ability of p53^{SM} 1-360 to bind to BCL-xLΔLΔC that is additionally bound to BH3 peptides other than PUMA^{BH3}. **a-b**. Overlaid ^{1}H-^{15}N TROSY spectra of 100 μM ^{15}N-BCL-xLΔLΔC in complex with unlabeled BAD^{BH3} (**a**) or BID^{BH3} (**b**) before (blue) and after (red) the addition of 1.5 molar excess p53^{SM} 1-360. The significant peak broadening observed upon addition of p53^{SM} 1-360 indicates interactions between this protein and ^{15}N-BCL-xLΔLΔC within the two BH3 peptide complexes.

Supplementary Figure 12

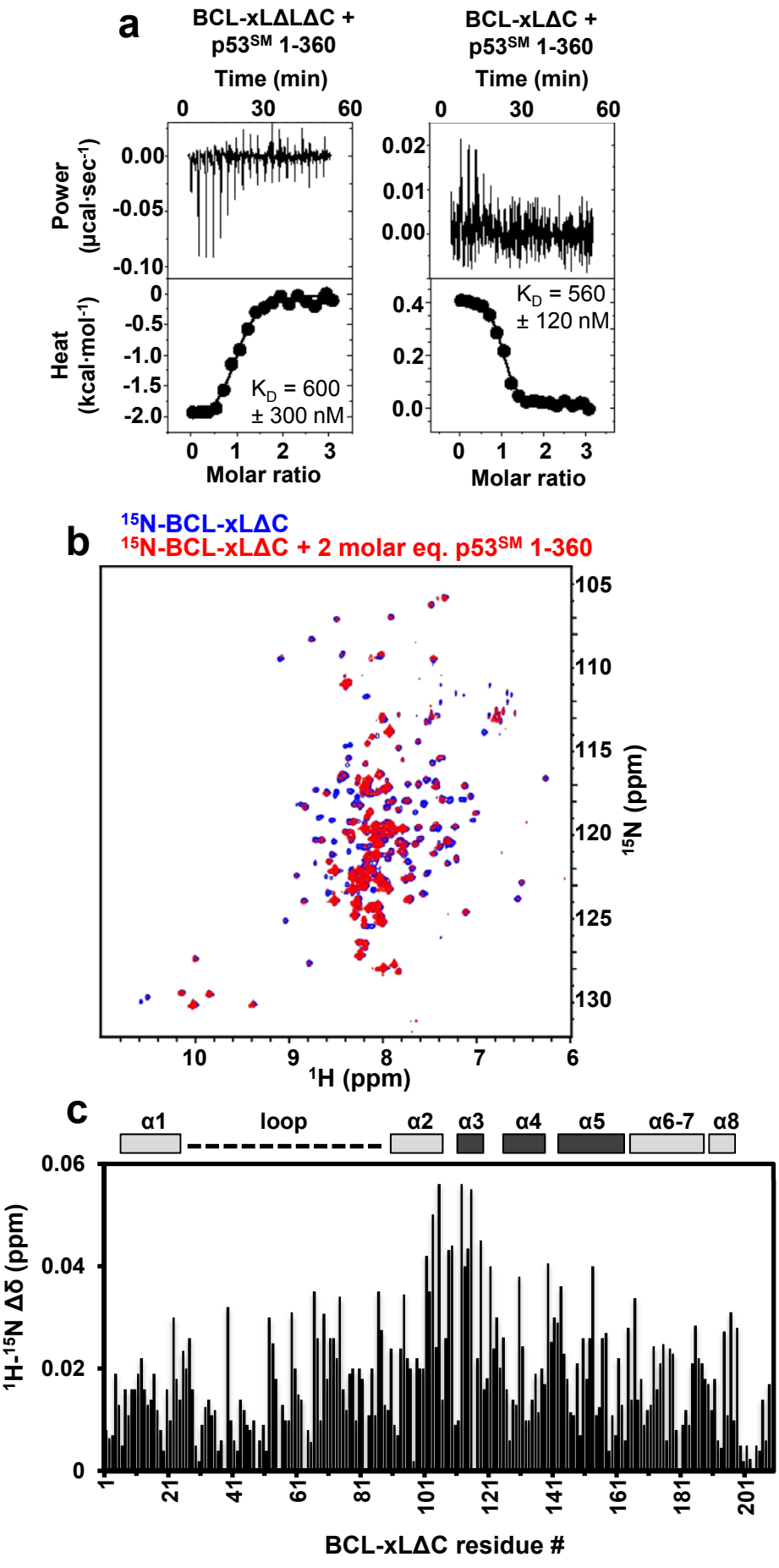

Supplementary Figure 12 (previous page). The two BCL-xL constructs, BCL-xLΔLΔC and BCL-xLΔC, bind similarly to $p53^{SM}$ 1-360. **a**. ITC binding isotherms for BCL-xLΔLΔC and BCL-xLΔC (200 μM) titrated into a solution of $p53^{SM}$ 1-360 (20 μM). The interaction of $p53^{SM}$ 1-360 with the two BCL-xL constructs is characterized by very small enthalpy values of opposite sign due to different degrees of enthalpy-entropy compensation; however, the K_D values determined through fitting these isotherms to a 1:1 binding model are nearly identical, and in good agreement with the values obtained from fluorescence polarization experiments (Suppl. Fig. 7). Errors represent the standard deviation calculated from at least two independent experiments. **b**. ^{1}H-^{15}N NMR chemical shift perturbation of ^{15}N-BCL-xLΔC upon binding by $p53^{SM}$ 1-360. 2D ^{1}H-^{15}N TROSY spectra of ^{15}N-BCL-xLΔC were recorded in the absence (blue colored peaks) and presence (red colored peaks) of a 2 molar excess of $p53^{SM}$ 1-360. **c**. ^{1}H-^{15}N NMR chemical shift perturbation analysis of the data presented in **c** for $p53^{SM}$ 1-360 binding to ^{15}N-BCL-xLΔLΔC. These data are consistent with the chemical shift perturbations observed for ^{15}N-BCL-xLΔLΔC upon binding of $p53^{SM}$ 1-360 (Suppl. Fig. 10).

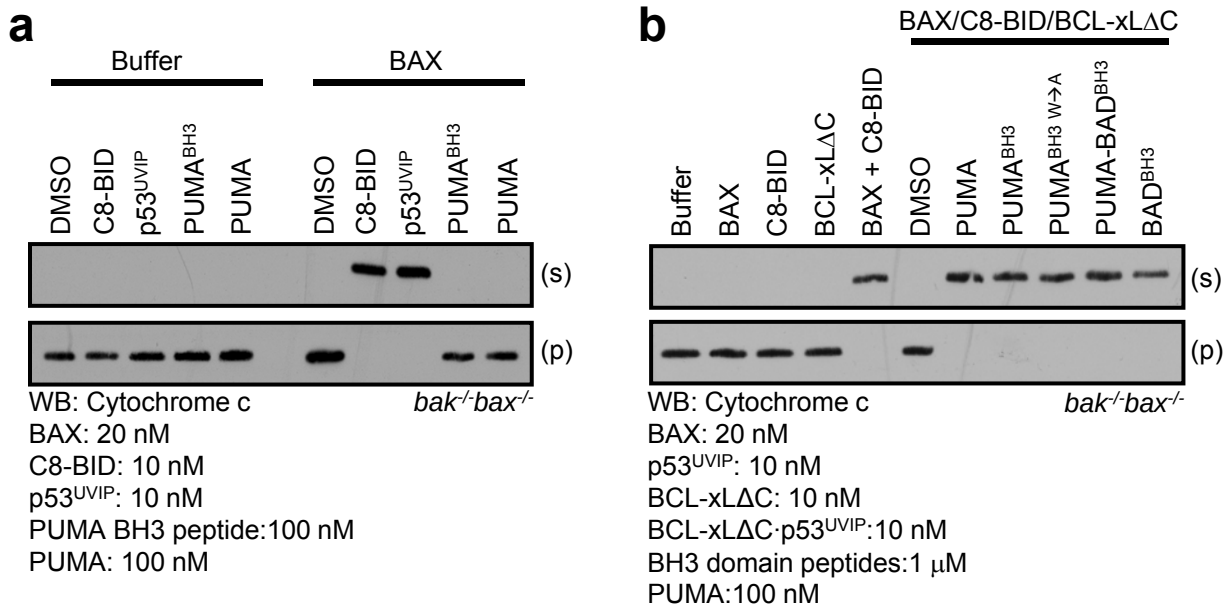

Supplementary Figure 13. p53 and C8-BID are direct activators of BAX-dependent MOMP while PUMA functions through de-repression of BCL-xL-inhibited C8-BID or p53 (shown in Fig. 3c). **a**. Purified mitochondria from *bak*$^{-/-}$ *bax*$^{-/-}$ liver were treated with p53^{UVIP} or C8-BID in the presence of BAX before fractionation, SDS-PAGE and western blot analyses for cytochrome c. C8-BID was a positive control for direct activator function. **b**. PUMA^{BH3} Trp^{71} was not critical for de-repression of C8-BID from BCL-xL. BCL-xLΔC·C8-BID complexes were combined with *bak*$^{-/-}$*bax*$^{-/-}$ liver mitochondria in the presence of BAX and indicated de-repressor BH3 domain peptides or PUMA before fractionation, SDS-PAGE and western blot analyses for cytochrome c. Mitochondrial cytochrome c, “p”; released cytochrome c, “s”.

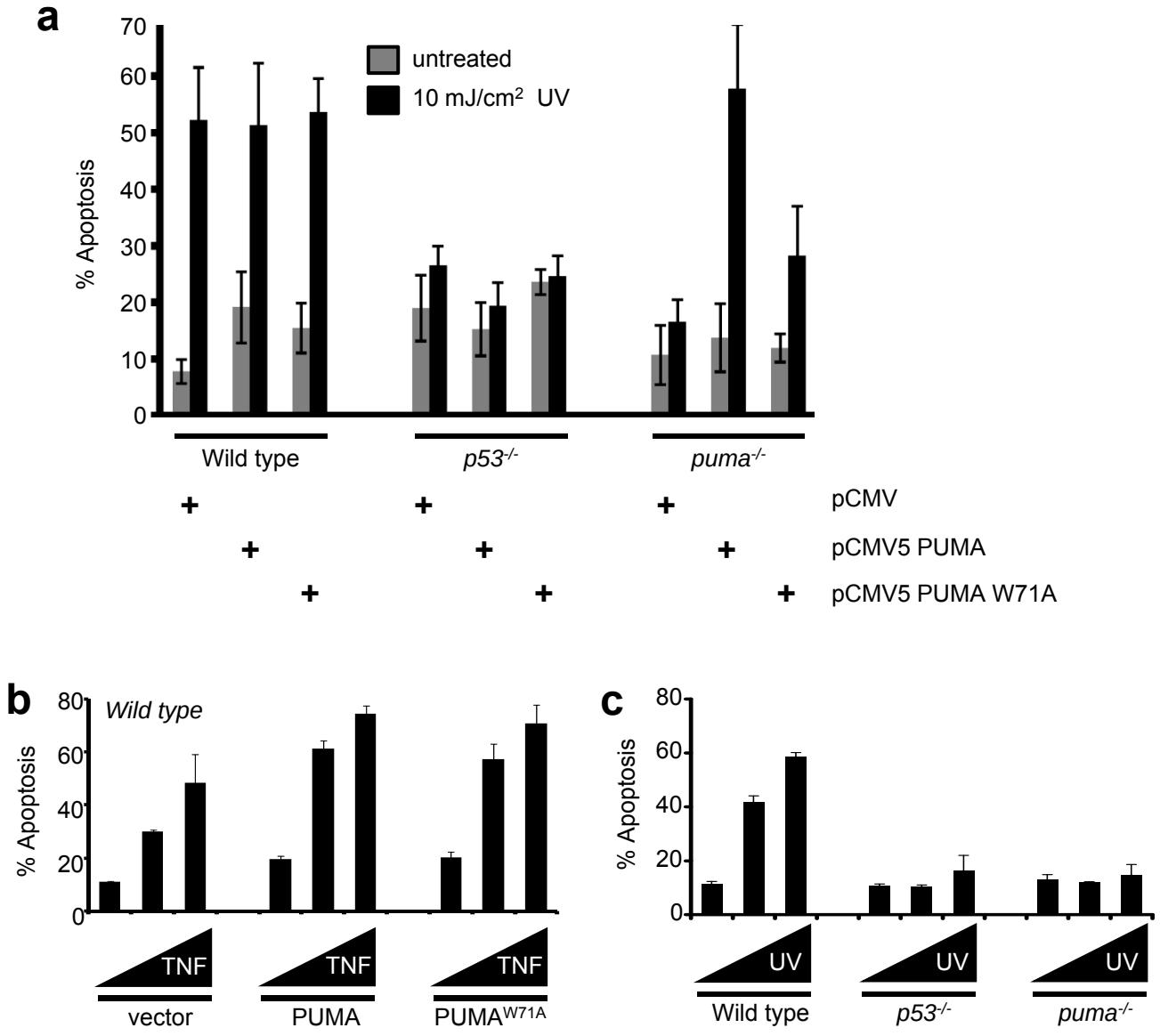

Supplementary Figure 14. Wild-type PUMA, but not PUMA$^{W\rightarrow A}$, induces apoptosis in a p53-dependent manner. **a**. Wild-type, *p53*$^{-/-}$ and *puma*$^{-/-}$ MEFs were transiently transfected with pCMV, pCMV5neoBam-FLAG-PUMA or pCMV5neoBam-FLAG-PUMA W71A (PUMA W71A) using 50 ng plasmid and Lipofectamine 2000, allowed to recover for 24 h, treated with UV irradiation (0 or 10 mJ/cm^2) and analyzed 24 hours later by AnnexinV-PE staining and flow cytometry for apoptosis. US9-GFP was co-transfected and only GFP positive cells were analyzed. Error bars represent the standard deviation from triplicate studies. **b**. Wild type MEFs were transfected as described above, treated with TNF (0, 5 & 10 ng/ml) and cycloheximide (10 μg/ml) for 6 hours and analyzed for apoptosis. US9-GFP was co-transfected and only GFP positive cells were analyzed. **c**. Wild type, *p53*$^{-/-}$ and *puma*$^{-/-}$ MEFs were treated with UV irradiation (0, 2.5 & 5 mJ/cm^2) and analyzed 24 hours later for apoptosis.

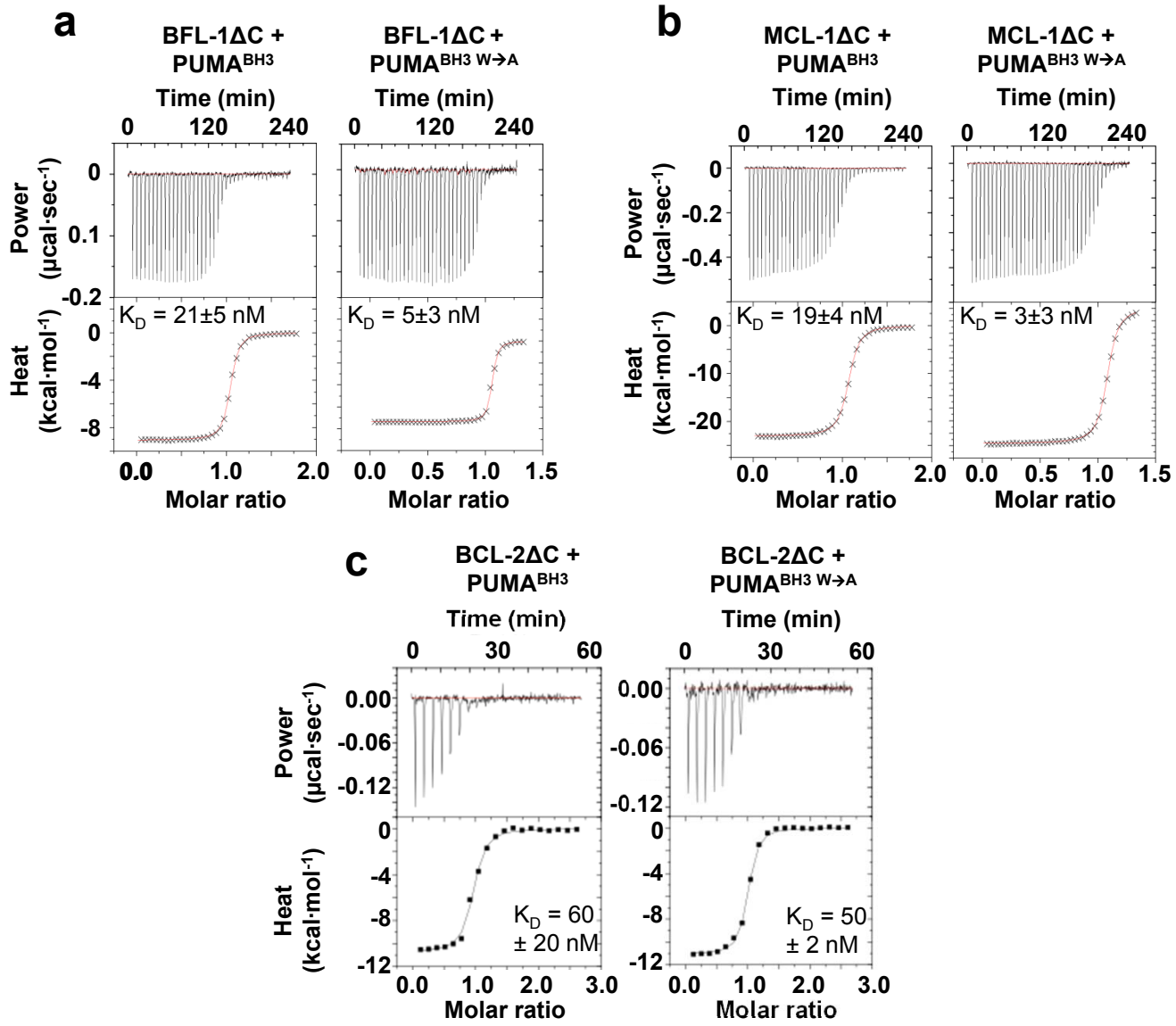

Supplementary Figure 15. The Trp^{71} to Ala mutation in PUMA^{BH3} (PUMA$^{BH3\ W\rightarrow A}$) does not significantly affect binding to anti-apoptotic BCL-2 family proteins other than BCL-xL. ITC binding isotherms for PUMA^{BH3} and PUMA$^{BH3\ W\rightarrow A}$ (100 μM) titrated into a solution of BFL-1ΔC (10 μM) (**a**), MCL-1ΔC (10 μM) (**b**), or BCL-2ΔC (**c**). Errors represent the standard deviation calculated from at least two independent experiments.

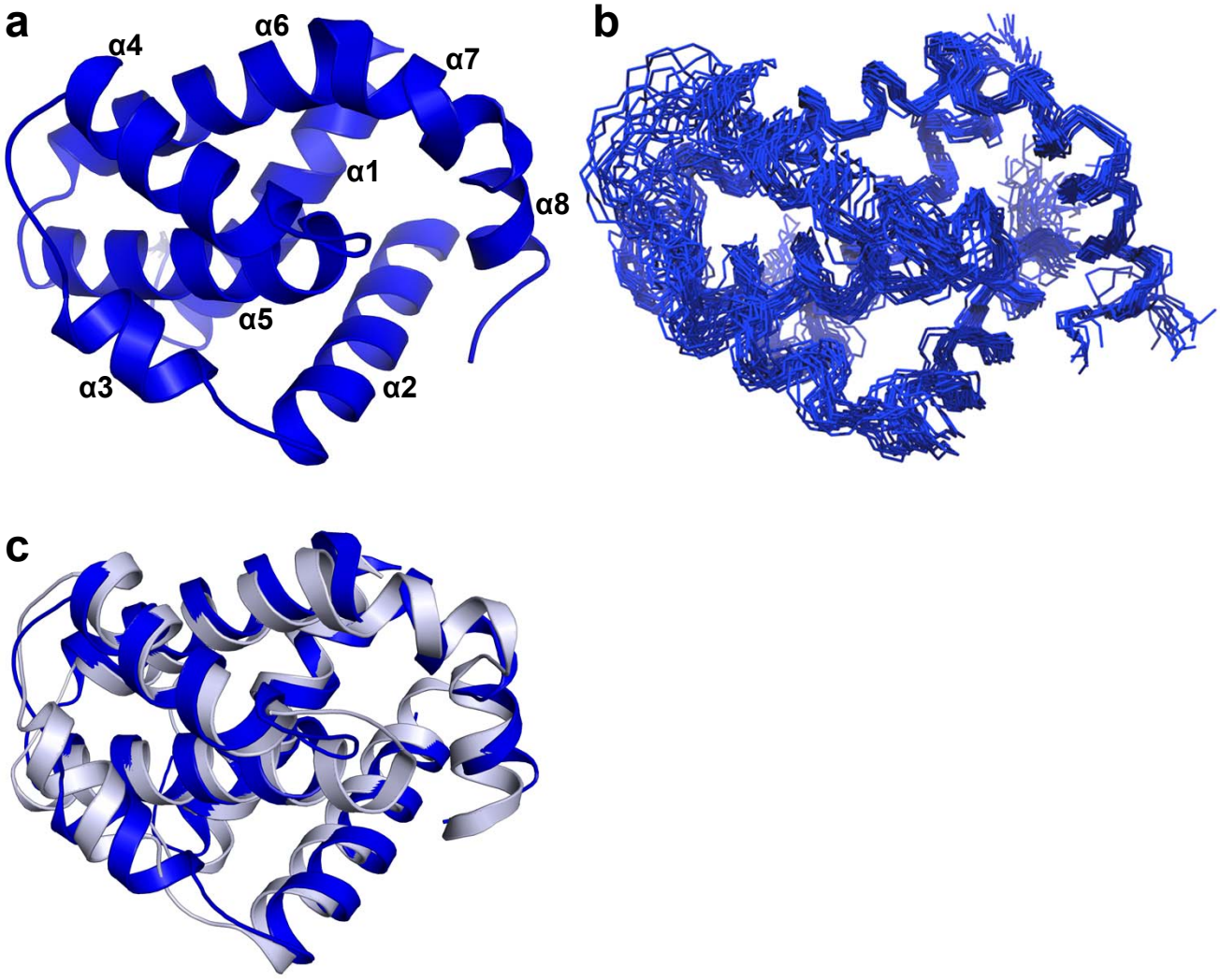

Supplementary Figure 16. NMR solution structure of free BCL-xLΔLΔC calculated using ^{15}N,^{13}C, ^{2}H-labeled protein with selective protonation of Ile, Leu, Val methyl moieties. **a**. Cartoon representation of the lowest-energy structure. **b**. Backbone atom representation of the aligned 20 lowest-energy structures. **c**. Structural alignment between the lowest-energy structure (dark blue) and the x-ray structure of BCL-xLΔC (light blue; PDB: 1R2D). The heavy atom backbone r.m.s.d. between the two models is 2.06 Å.

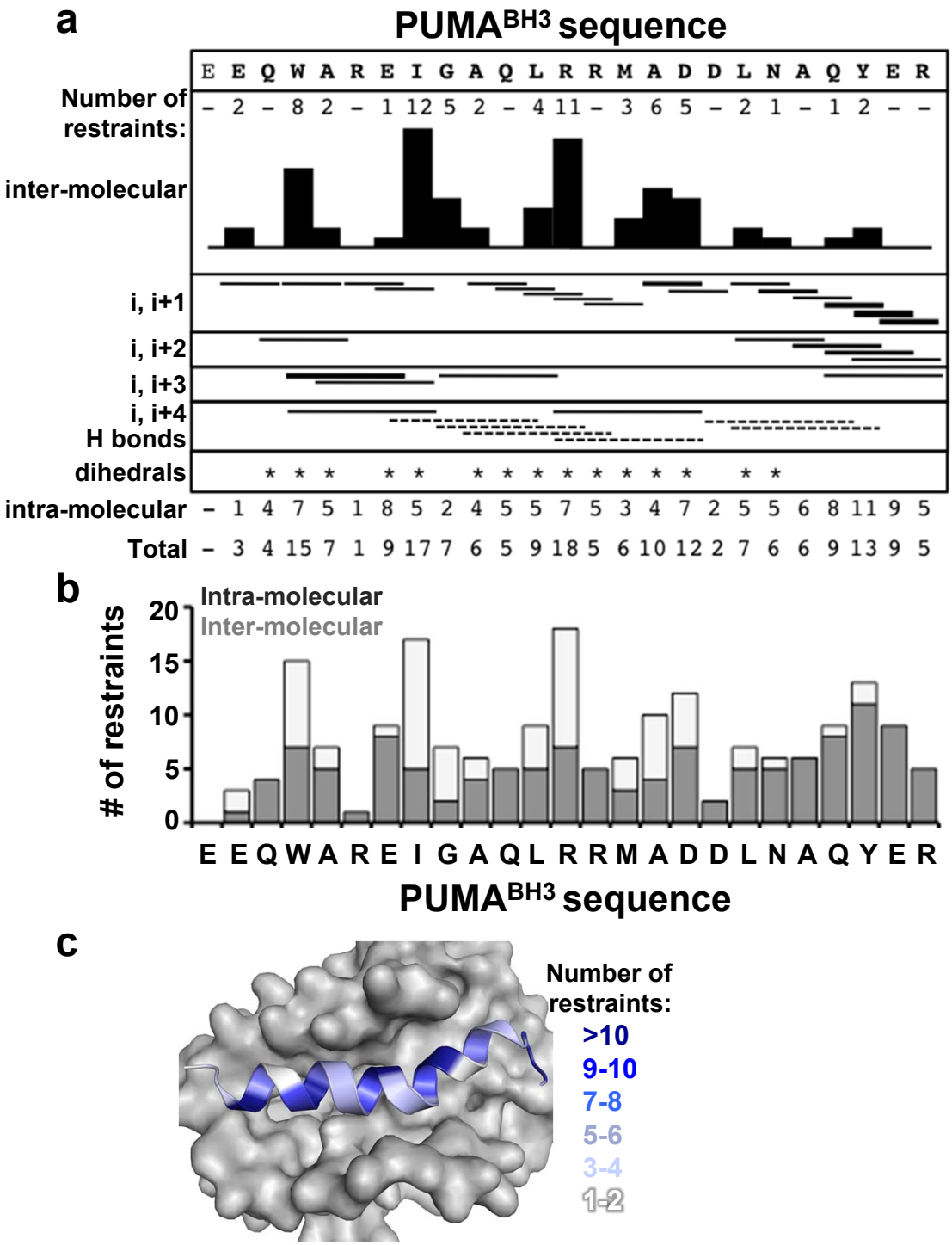

Supplementary Figure 17. Summary of NMR-derived distance restraints applied to the PUMA^{BH3} peptide during calculation of the solution structure of the BCL-xLΔLΔC·PUMA^{BH3} complex. **a**. Sequence mapping of inter-residue distance restraints. The number of inter-molecular restraints (to BCL-xLΔLΔC) is indicated in the bar plot at the top of the panel. The line thickness is proportional to the number of restraints between pairs of residues. **b**. Bar plot representation of the overall per-residue restraint density. **c**. Color coded structure mapping of the restraint density. Dark blue coloring indicates a larger number of restraints, light blue fewer restraints.

Figure 3a

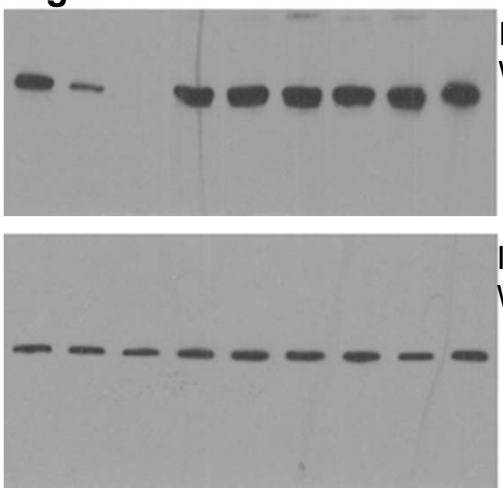

Figure 3b

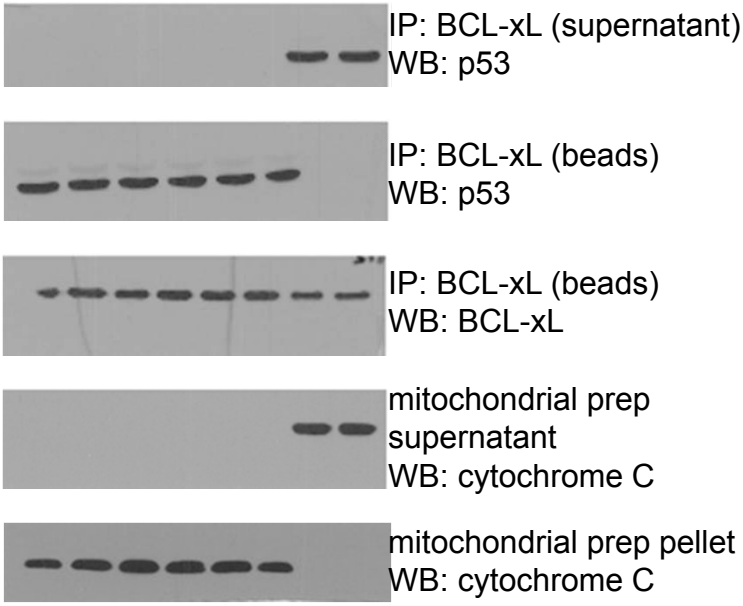

Figure 3c

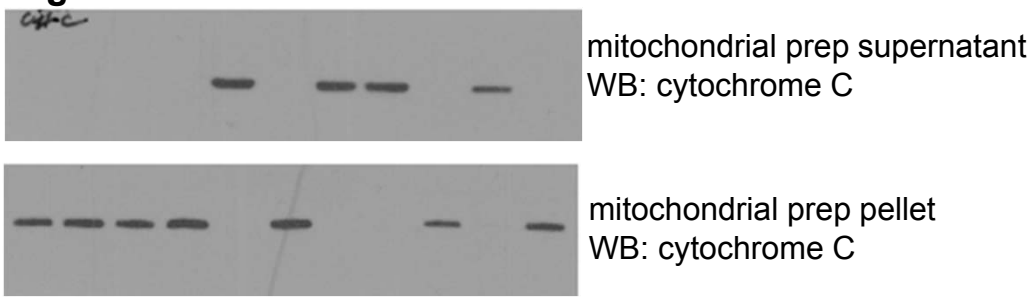

Figure 4c

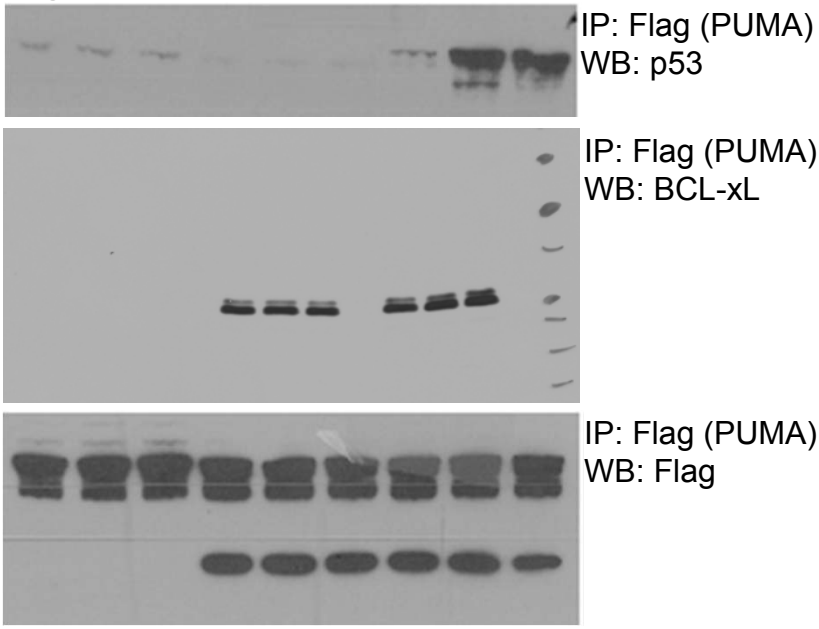

Supplementary Figure 18. Full-size views of western blot films displayed in a cropped format in Figures 3 and 4, as indicated nearby each panel. The blot of BCL-xL in Figure 4c has a different lane spacing compared to that of the corresponding p53 and PUMA blots because the IP samples were analyzed using a second SDS-PA gel, which was then western blotted for BCL-xL. This second gel was run using 15 *versus* 12 lanes, with a blank lane between each set of three experimental samples, as was used for the gel for analysis of p53 and PUMA (Flag).

Supplementary Table 1. NMR solution structure statistics

	BCL-xLΔLΔC	BCL-xLΔLΔC·PUMA^{BH3}
NMR distance and dihedral constraints		
Distance constraints		
Total NOE	524	762
Intra-residue	40	86 (28)*
Inter-residue	484	676
Sequential ($\|i-j\|=1$)	189	235 (13)*
Medium-range ($\|i-j\|<4$)	186	246 (15)*
Long-range ($\|i-j\|>5$)	109	120
Intermolecular	----	75
Hydrogen bonds	70	79 (6)*
Total dihedral angle restraints	229	214
ϕ	**115**	**107**
ψ	**114**	**107**
Structure statistics		
Violations (mean and s.d.)		
Distance constraints (Å)	0.017±0.002	0.010±0.002
Dihedral angle constraints (º)	0.57±0.15	0.35±0.12
Max. dihedral angle violation (º)	4.66±2.64	2.55±1.02
Max. distance constraint violation (Å)	0.29±0.07	0.26±0.11
Deviations from idealized geometry		
Bond lengths (Å)	0.012	0.013
Bond angles (º)	1.6	1.7
Impropers (º)	----	----
Average pairwise r.m.s. deviation** (Å)		
Heavy	1.71±0.28	1.51±0.14
Backbone	1.01±0.26	0.93±0.14

*Values in parenthesis indicate intra-molecular restraints within the PUMA^{BH3} peptide
**Pairwise r.m.s. deviation was calculated among 20 refined structures for the alignment of the following well restrained segments: residues 1-21,23-26,84-100,103-111,120-132,137-158,162-194, 199-203(BCL-xLΔLΔC); residues 3-20,82-96,110-113,118-132,136-176,178-185,188-195, puma 70-91 (BCL-xLΔLΔC·PUMA^{BH3}).

Supplementary Table 2. Data collection and refinement statistics (**Molecular Replacement**)

	BCL-xL·PUMA^{BH3}
Data collection	
Space group	$P4_22$
Cell dimensions	
a, *b*, *c* (Å)	94.8, 94.8, 111.5
α, β, γ (°)	90.0, 90.0, 90.0
Resolution (Å)	50-2.9 (3.0-2.9)*
R_{sym}	9.4 (38)
$I / \sigma I$	38.5 (3.3)
Completeness (%)	96.0 (68.9)
Redundancy	21.7 (8.8)
Refinement	
Resolution (Å)	42.9-2.9
No. reflections	11256
R_{work} / R_{free}	0.206/0.254
No. atoms	
Protein	2330
Ligand/ion	0
Water	4
B-factors	
Protein	93.9
Ligand/ion	-----
Water	67.7
R.m.s. deviations	
Bond lengths (Å)	0.004
Bond angles (°)	0.775

The structure was determined from diffraction of a single crystal.
*Highest-resolution shell is shown in parentheses.

Supplementary Table 3. Results of analytical ultracentrifugation sedimentation experiment

Sample	S_{20} (Svedberg)[a]	$S^0_{20,w}$ (Svedberg)[b]	M (Da)[c]	f/f_0[d]
BCL-xL ΔLΔC	2.02 (92%)	2.12	21,100 (20,650)	1.37 (1.34)
BCL-xL ΔLΔC ·PUMA^{BH3}	2.26 (92%)	2.38	24,700 (23,681)	1.39 (1.32)

[a] Sedimentation coefficient taken from the ordinate maximum of each peak in the best-fit *c(s)* distribution at 20 °C with percentage protein amount in parenthesis. Sedimentation coefficient (*s*-value) is a measure of the size and shape of a protein in a solution with a specific density and viscosity at a specific temperature.
[b] Standard sedimentation coefficient ($s^0_{20,w}$-value) at zero concentration, in water at 20 °C.
[c] Molar mass values taken from the *c(s)* distribution that was transformed to the *c(M)* distribution. The theoretical mass of the monomer is given in parenthesis.
[d] Best-fit weight-average frictional ratio values $(f/f_0)_w$ taken from the *c(s)* distribution. The frictional ratios calculated with $s^0_{20,w}$-values via the v-bar method (SEDNTERP) is in parenthesis.

Supplementary Table 4. Results of analytical ultracentrifugation equilibrium experiment

Sample	K_D (nM)	r.m.s.d.
BCL-xL ΔLΔC ·PUMA^{BH3}	10-30	0.0029

Supplementary Table 5. Values of equilibrium dissociation constants (K_D) for BCL-xLΔC binding to a panel of BH3 peptides determined by iosthermal titration calorimetry (ITC). Error bars represent the standard deviation calculated from at least two independent experiments.

BH3 peptide	K_D (nM)
BAD	0.2±0.3
BAK	28±3
BAX	120±75
BID	10±15
BIM	1±7
HRK	30±35
Noxa	ND
PUMA	3±2
PUMA$^{W\rightarrow A}$	3±1

Supplementary References

1 Muchmore, S. W. *et al.* X-ray and NMR structure of human Bcl-xL, an inhibitor of programmed cell death. *Nature* **381**, 335-341 (1996).

2 Denisov, A. Y., Sprules, T., Fraser, J., Kozlov, G. & Gehring, K. Heat-induced dimerization of BCL-xL through alpha-helix swapping. *Biochemistry* **46**, 734-740 (2007).

3 Sattler, M. *et al.* Structure of Bcl-xL-Bak peptide complex: recognition between regulators of apoptosis. *Science* **275**, 983-986 (1997).

4 Petros, A. M. *et al.* Rationale for Bcl-xL/Bad peptide complex formation from structure, mutagenesis, and biophysical studies. *Protein Sci* **9**, 2528-2534 (2000).

5 Feng, W., Huang, S., Wu, H. & Zhang, M. Molecular basis of Bcl-xL's target recognition versatility revealed by the structure of Bcl-xL in complex with the BH3 domain of Beclin-1. *J Mol Biol* **372**, 223-235 (2007).

6 Liu, X., Dai, S., Zhu, Y., Marrack, P. & Kappler, J. W. The structure of a Bcl-xL/Bim fragment complex: implications for Bim function. *Immunity* **19**, 341-352 (2003).

7 Petros, A. M., Gunasekera, A., Xu, N., Olejniczak, E. T. & Fesik, S. W. Defining the p53 DNA-binding domain/Bcl-x(L)-binding interface using NMR. *FEBS Lett* **559**, 171-174 (2004).